European Polymer Journal 109 (2018) 206–213

Contents lists available at ScienceDirect

European Polymer Journal

journal homepage: www.elsevier.com/locate/europolj

Collisional lipid exchange among DIBMA-encapsulated nanodiscs (DIBMALPs)

Bartholomäus Danielczak, Sandro Keller*

Molecular Biophysics, Technische Universität Kaiserslautern (TUK), Erwin-Schrödinger-Str. 13, 67663 Kaiserslautern, Germany

ARTICLE INFO

Keywords:
Davies equation
Debye–Hückel theory
DIBMALPs
Polymer nanodiscs
Lipid transfer

ABSTRACT

Copolymers of diisobutylene/maleic acid (DIBMA), styrene/maleic acid (SMA), and styrene/maleimide (SMI) solubilise membrane proteins and surrounding lipids directly from artificial and biological membranes to form polymer-bounded nanodiscs. Although they preserve a lipid-bilayer core, these nanodiscs are much more dynamic than other membrane mimics, as we have recently demonstrated for two SMA variants. Here, we used time-resolved Förster resonance energy transfer spectroscopy to quantify the kinetics and unravel the mechanisms of lipid transfer among DIBMA-encapsulated nanodiscs (DIBMALPs), with particular emphasis on the role of Coulombic repulsion, which is modulated by ionic strength and nanodisc size. Our results show that DIBMALPs exchange lipids through both binary and ternary collisions on the timescale of seconds to minutes under typical experimental conditions. By contrast, nanodiscs bounded by SMA polymers exchange lipids considerably faster through binary collisions, whereas vesicles and nanodiscs based on membrane scaffold proteins exchange lipids much more slowly through lipid monomer diffusion. As DIBMALPs are polyanionic, collisional lipid transfer is substantially accelerated by screening of Coulombic repulsion caused by increasing ionic strength or nanodisc size. Analysis of the ionic-strength dependence in terms of an extended version of the Debye–Hückel equation suggests an effective DIBMALP charge number of $z = -47$, which is considerably larger than that previously determined for nanodiscs bounded by more hydrophobic SMA polymers.

1. Introduction

Amphiphilic copolymers of diisobutylene/maleic acid (DIBMA) [1,2], styrene/maleic acid (SMA) [3,4], and styrene/maleimide (SMI) [5] have attracted great attention because they can directly extract and stabilise membrane proteins in a supposedly near-native lipid-bilayer environment without requiring conventional detergents [1,4,6,7]. Along with membrane proteins, these polymers can co-extract surrounding lipid molecules from artificial or biological membranes to form polymer-bounded nanodiscs that preserve an intact lipid-bilayer core. Membrane proteins extracted into polymer-encapsulated nanodiscs may then be studied through a wide range of biophysical [1,8,9], structural [10–13], and functional approaches [1,14–17].

In spite of their high thermodynamic and colloidal stability, polymer-bounded nanodiscs represent highly dynamic rather than static, kinetically trapped lipid assemblies. In particular, several lines of evidence have demonstrated that SMA/lipid particles (SMALPs) readily exchange proteins, lipids, and polymer chains among each other and with other membrane mimics. For instance, single copies of an ion-channel protein have been transferred from SMALPs to planar lipid membranes for electrophysiological experiments [9], while *en masse* transfer of another membrane protein from SMALPs to lipidic cubic phases has been established to grow crystals for X-ray scattering [11]. Evidence has been found for lipid exchange between SMALPs and lipid monolayers [18] as well as for the re-integration of SMA-solubilised phospholipids into large unilamellar vesicles (LUVs) [19]. Finally, Schmidt and Sturgis have shown rapid exchange of fluorescently labelled polymer chains among SMALPs [20].

We have recently demonstrated that, owing to efficient collisional transfer, lipids exchange rapidly among nanodiscs encapsulated by SMA(3:1) [21], with observed rate constants several orders of magnitude larger than found for conventional bilayer-preserving membrane mimics such as LUVs [22] and nanodiscs bounded by membrane scaffold protein (MSP) [23]. Even on an absolute scale, the observed lipid transfer is remarkably fast considering the polyanionic nature of SMALPs and the ensuing Coulombic repulsion that must be overcome for collisional content exchange. We have reported similar findings [24] for a less hydrophobic and even more charged polymer variant, namely, SMA(2:1), which is a more efficient solubiliser of lipids [25] and proteins [26,27]. As expected, lipid transfer is significantly slower for

* Corresponding author.
E-mail address: mail@sandrokeller.com (S. Keller).

https://doi.org/10.1016/j.eurpolymj.2018.09.043
Received 2 July 2018; Received in revised form 24 August 2018; Accepted 21 September 2018
Available online 22 September 2018
0014-3057/

SMA(2:1) than for SMA(3:1) but is still orders of magnitude faster than among LUVs or MSP nanodiscs. Moreover, lipid transfer among SMA-encapsulated nanodiscs can be accelerated drastically by raising the ionic strength of the buffer. Analysis of this Coulombic-screening effect in terms of an extended version of the Debye–Hückel equation suggests an effective charge of SMA(2:1)-encapsulated nanodiscs of –33 elementary charges [24].

DIBMA represents a milder alternative to SMA that better preserves the order and dynamics of extracted lipids [1,2,25]. This is presumably due to, at least partly, the lower hydrophobicity of DIBMA, which means that this polymer carries an even higher charge density than common SMA variants. This property as well as the preservation of a tightly packed lipid-bilayer core in DIBMALPs are expected to slow down both diffusional and collisional lipid transfer. An important feature of DIBMALPs is their size tunability, which is possible through changes in the DIBMA/lipid ratio. Furthermore, as changes in size are accompanied by shifts in the number and density of anionic groups at the nanodisc rim, the kinetics of lipid transfer may depend on the size of the DIBMALPs used.

To address these points, we quantified the kinetics and unravelled the mechanisms of lipid transfer among DIBMALPs. In doing so, we paid particular attention to the role of Coulombic repulsion, which, in turn, depends on ionic strength and nanodisc size. To this end, we used time-resolved Förster resonance energy transfer (TR-FRET) spectroscopy to monitor the lipid-transfer kinetics among DIBMALPs containing the zwitterionic phospholipid 1,2-dimyristoyl-*sn*-glycero-3-phosphocholine (DMPC) at different ionic strengths and nanodisc sizes. We find that DIBMALPs exchange lipids mainly through collisions between two or among three nanodiscs, which sets them apart from other polymer-based nanodiscs and more conventional membrane mimics. Moreover, lipid transfer among DIBMALPs is strongly accelerated by increasing the ionic strength or the size of the nanodiscs.

2. Experimental section

2.1. Materials

DIBMA (Sokalan CP 9, $M_n = 8.4\,\mathrm{kg\,mol^{-1}}$, $M_w = 15.3\,\mathrm{kg\,mol^{-1}}$) and DMPC were kindly provided by BASF (Ludwigshafen, Germany) and Lipoid (Ludwigshafen, Germany), respectively. *N*-(7-nitrobenz-2-oxa-1,3-diazol-4-yl)-1,2-dihexadecanoyl-*sn*-glycero-3-phosphoethanolamine (NBD-PE) and *N*-(lissamine rhodamine B sulfonyl)-1,2-dihexadecanoyl-*sn*-glycero-3-phosphoethanolamine (Rh-PE) were purchased from Fisher Scientific (Schwerte, Germany) and Biotium (Fremont, USA), respectively. Tris(hydroxymethyl)aminomethane (Tris) was from Carl Roth (Karlsruhe, Germany), NaOH from Sigma–Aldrich (Steinheim, Germany), NaCl from VWR (Darmstadt, Germany), and $CHCl_3$ from Fisher Scientific. All chemicals were purchased in the highest purity available.

2.2. Preparation of DIBMA stock solution

3 mL of a commercial DIBMA solution was placed into a 5-mL QuixSep microdialysis capsule (Carl Roth) and dialysed using a Spectra/Por 3 dialysis membrane (Spectrum Laboratories, Rancho Dominguez, USA) with a nominal molar-mass cutoff of $3.5\,\mathrm{kg\,mol^{-1}}$. Dialysis was performed at room temperature against 1 L of buffer (50 mM Tris, 100 mM NaCl, pH 7.4) for 24 h with buffer exchange after 16 h. Then, the DIBMA stock solution was sterile-filtered through a syringe filter (Carl Roth) with a nominal pore diameter of 220 nm. The DIBMA concentration was determined refractometrically on an Abbemat 500 (Anton Paar, Graz, Austria) using $dn/dc = 1.346\,\mathrm{M^{-1}}$ based on M_n [1].

2.3. Preparation of DIBMALPs

For fluorescently labelled DIBMALPs, DMPC, NBD-PE, and Rh-PE powders were separately dissolved in $CHCl_3$ before mixing at a molar ratio of 98:1:1. A thin lipid film was obtained after solvent removal using a Rotavapor R-210 evaporator (Büchi, Essen, Germany). Trace amounts of solvent were removed under high vacuum in a desiccator for at least 16 h. Lipid films were suspended in buffer (50 mM Tris, 100 mM NaCl, pH 7.4) by vortexing at 35 °C before at least six freeze–thaw cycles were performed. Because DIBMALPs decrease in size with increasing ionic strength [2] or increasing polymer/lipid ratio [1,2], the latter was adjusted such as to afford the same nanodisc size across all NaCl concentrations. Specifically, lipid suspensions having final concentrations of $c_L = 5$ mM were solubilised with 0.65 mM, 0.46 mM, 0.31 mM, and 0.28 mM DIBMA at $c_{NaCl} = 100$ mM, 200 mM, 400 mM, and 600 mM, respectively. In all cases, solubilisation at 35 °C with gentle agitation for ~16 h yielded DIBMALPs with z–averaged hydrodynamic diameters and associated size-distribution widths of $d_z = (23 \pm 3)$ nm. To generate DIBMALPs with $d_z = (32 \pm 2)$ nm and (40 ± 2) nm at 200 mM NaCl, the polymer concentration was lowered to $c_{DIBMA} = 0.34$ mM and 0.30 mM, respectively. For unlabelled DIBMALPs, the same lipid/polymer ratios were used at a total lipid concentration of $c_L = 40$ mM, from which nanodiscs were diluted to final lipid concentrations of $c_L = 30$, 20, 10, 5, 2.5, and 1 mM. For all samples, unimodal nanodisc size distributions were confirmed by dynamic light scattering (DLS). Inclusion of 1 mol% of each of the two fluorescently labelled lipids had no effect on particle size distributions as compared with those of DIBMALPs containing only DMPC, as also found earlier [21,24].

2.4. DLS

DLS measurements were carried out on a Zetasizer Nano S90 (Malvern Panalytical, Malvern, UK) equipped with a He–Ne laser emitting at 633 nm. Samples were measured in a 3 mm × 3 mm quartz cuvette (Hellma Analytics, Müllheim, Germany) thermostatted at 30 °C using automated laser attenuation. z-Average diameters and associated size-distribution widths were obtained from cumulant analysis of autocorrelation functions [28].

2.5. TR-FRET

Measurements were carried out on an SF.3 stopped-flow apparatus (Applied Photophysics, Leatherhead, UK) equipped with a (470 ± 10) nm light-emitting diode, whose output was set to (2–20) mA and further attenuated by an OD 2 filter (Applied Photophysics) to avoid photobleaching. Fluorescence emission was blocked below 513 nm and above 543 nm with a TechSpec OD 6 band-pass filter (Edmund Optics, Karlsruhe, Germany) and was monitored using a photomultiplier mounted at a right angle. Drive syringes, tubes, and the quartz glass cell were thermostatted at 30 °C at all times. Samples were equilibrated for at least 10 min prior to each measurement. Then, 75-μL aliquots of fluorescently labelled DIBMALPs at $c_L = 0.5$ mM were mixed rapidly with equal volumes of unlabelled DIBMALPs at $c_L = 40$, 30, 20, 10, 5, 2.5, and 1 mM. For each c_L and c_{NaCl}, the time-dependent emission from NBD-PE was recorded 4–10 times with 10′000 data points per shot. The fluorescence transients thus obtained were averaged and analysed by nonlinear least-squares fitting [29].

3. Theoretical background

3.1. Lipid-transfer kinetics among DIBMALPs

Nanoparticles may exchange lipids through (i) desorption of lipid monomers and interparticle diffusion through the aqueous phase [30–32] and (ii) collisions between two or among more nanoparticles

[33–36]. If the size and the shape of the lipid-exchanging particles are identical, the observed rate constant due to diffusional lipid exchange is given by [33,34,36]:

$$k_{\mathrm{obs,dif}}(c_{\mathrm{L}}) = \frac{k_{\mathrm{dif}}\, c_{\mathrm{L}}}{c_{\mathrm{L}}^{\circ} + c_{\mathrm{L}}} \tag{1}$$

where k_{dif} is the diffusional lipid-exchange rate constant and c_{L}° and c_{L} are the total lipid concentrations initially in the donor and acceptor nanodisc populations, respectively. For collision-dependent lipid transfer between two or among three particles, the observed rate constants amount to, respectively:

$$k_{\mathrm{obs,bi}}(c_{\mathrm{L}}) = k_{\mathrm{bi}}\, c_{\mathrm{L}} \tag{2}$$

and

$$k_{\mathrm{obs,ter}}(c_{\mathrm{L}}) = k_{\mathrm{ter}}\, c_{\mathrm{L}}^{2} \tag{3}$$

where k_{bi} and k_{ter} are the second-order and third-order rate constants characterising lipid exchange through binary and ternary collisions, respectively. If all of the above mechanisms contribute to lipid transfer, the overall observed rate constant is given by the sum of Eqs. (1), (2), and (3) [33,34,36]:

$$k_{\mathrm{obs}}(c_{\mathrm{L}}) = k_{\mathrm{obs,dif}}(c_{\mathrm{L}}) + k_{\mathrm{obs,bi}}(c_{\mathrm{L}}) + k_{\mathrm{obs,ter}}(c_{\mathrm{L}}) = \frac{k_{\mathrm{dif}}\, c_{\mathrm{L}}}{c_{\mathrm{L}}^{\circ} + c_{\mathrm{L}}} + k_{\mathrm{bi}}\, c_{\mathrm{L}} + k_{\mathrm{ter}}\, c_{\mathrm{L}}^{2} \tag{4}$$

3.2. Dependence on lipid concentration

Mixing labelled and unlabelled DIBMALPs leads to a redistribution and dilution of NBD-PE and Rh-PE. This process increases the average distance between the fluorophores and, thus, reduces donor quenching. Consequently, the fluorescence emission intensity of NBD-PE at 530 nm increases exponentially:

$$F(t) = F_{\infty} + e^{-k_{\mathrm{obs}}\, t}(F_0 - F_{\infty}) \tag{5}$$

Here, $F(t)$ is the intensity at time t after mixing, and F_0 and F_{∞} are the original and final intensities, respectively. For global data analysis, Eq. (4) was inserted into Eq. (5) to yield:

$$F(t) = F_{\infty} + e^{-\left(\frac{k_{\mathrm{dif}}\, c_{\mathrm{L}}}{c_{\mathrm{L}}^{\circ} + c_{\mathrm{L}}} + k_{\mathrm{bi}}\, c_{\mathrm{L}} + k_{\mathrm{ter}}\, c_{\mathrm{L}}^{2}\right) t}(F_0 - F_{\infty}) \tag{6}$$

In this fitting equation, k_{dif}, k_{bi}, and k_{ter} are global fitting parameters, whereas F_0 and F_{∞} are local (i.e., c_{L}-specific) fitting parameters. Best-fit parameter values and 95% confidence intervals were derived by nonlinear least-squares fitting [29].

3.3. Dependence on ionic strength

According to the primary kinetic salt effect [37–39], k_{bi} depends on the ionic activity coefficient, γ, as expressed by:

$$\log\left(\frac{k_{\mathrm{bi}}}{\mathrm{M^{-1}s^{-1}}}\right) = \log\left(\frac{k_{\mathrm{bi}}^{0}}{\mathrm{M^{-1}s^{-1}}}\right) - 2\log(\gamma) \tag{7}$$

where k_{bi}^{0} is the hypothetical rate constant characterising lipid exchange through binary collisions at $\gamma = 1$, that is, at vanishing ionic strength.

Within the Debye–Hückel limit [40], γ depends on the ionic strength of the solution, I, according to:

$$\log(\gamma) = -Az^{2}\sqrt{I} \tag{8}$$

with $A = 0.516\ \mathrm{L^{1/2}\,mol^{-1/2}}$ at 30 °C [41]. Inserting Eq. (8) into Eq. (7) yields the Brønsted–Bjerrum equation [38,39]:

$$\log\left(\frac{k_{\mathrm{bi}}}{\mathrm{M^{-1}s^{-1}}}\right) = \log\left(\frac{k_{\mathrm{bi}}^{0}}{\mathrm{M^{-1}s^{-1}}}\right) + 2Az^{2}\sqrt{I} \tag{9}$$

Whereas the Debye–Hückel limiting law as embodied in Eq. (9) typically provides a reasonably good approximation only for $I \leq 10$ mM, the empirical extension suggested by Guggenheim [42] and Davies [43] holds also at higher c_{NaCl} up to 500 mM. The Davies equation [43] reads:

$$\log(\gamma) = -Az^{2}\left(\frac{\sqrt{I}}{1+\sqrt{I}} - 0.2I\right) \tag{10}$$

Using a factor of 0.3 instead of 0.2 in the last term of Eq. (10), as later suggested by Davies [44], had no significant effect on our best-fit values of z and k_{bi}^{0} (data not shown). Inserting Eq. (10) into Eq. (7) thus leads to a modified expression of the form:

$$\log\left(\frac{k_{\mathrm{bi}}}{\mathrm{M^{-1}s^{-1}}}\right) = \log\left(\frac{k_{\mathrm{bi}}^{0}}{\mathrm{M^{-1}s^{-1}}}\right) + 2Az^{2}\left(\frac{\sqrt{I}}{1+\sqrt{I}} - 0.2I\right) \tag{11}$$

Both the original Debye–Hückel limiting law and the Davies equation rely on point-charge assumptions. By contrast, another extension of the Debye–Hückel equation accounts for the finite size of the colliding particles, resulting in [41]:

$$\log(\gamma) = \frac{-Az^{2}\sqrt{I}}{1+Br\sqrt{I}} \tag{12}$$

with $B = 3.30\ \mathrm{nm^{-1}\ L^{1/2}\ mol^{-1/2}}$ at 30 °C and $r = 11.5$ nm being the DIBMALP radius. Again, inserting Eq. (12) into Eq. (7) leads to the following expression:

$$\log\left(\frac{k_{\mathrm{bi}}}{\mathrm{M^{-1}s^{-1}}}\right) = \log\left(\frac{k_{\mathrm{bi}}^{0}}{\mathrm{M^{-1}s^{-1}}}\right) + 2\frac{Az^{2}\sqrt{I}}{1+Br\sqrt{I}} \tag{13}$$

This equation is usually applicable only at low ionic strengths of $I \leq 100$ mM. Therefore, we tried replacing the $\sqrt{I}$ term in Eq. (12) by the Davies term in Eq. (10), which, however, had no significant effect on the best-fit values of z and k_{bi}^{0} (data not shown).

By utilising either Eq. (9), Eq. (11), or Eq. (13), best-fit parameter values of k_{bi}^{0} and z were derived by nonlinear least-squares fitting of k_{bi} as a function of I [29]. It should be noted that analogous considerations apply to the effect of ionic strength on ternary collisions. However, we refrained from a more detailed analysis of k_{ter} values because the latter were constrained less well by the experimental data. This was particularly true at high ionic strengths, where the contribution of ternary collisions was of minor importance even at the highest lipid concentrations tested (data not shown).

3.4. Diffusion-limited collisional lipid transfer

According to the Stokes–Einstein–Smoluchowski equation [45], the diffusion-limited upper bound on the binary collisional rate constant for non-ionic particles amounts to:

$$k_{\mathrm{bi,max}} = \frac{8RT}{3\eta} \tag{14}$$

where R denotes the universal gas constant, T the absolute temperature, and η the dynamic viscosity of the buffer.

4. Results and discussion

4.1. Lipid-transfer kinetics among DIBMALPs

Lipid transfer commonly takes place via two distinct mechanisms: (i) diffusional transfer of lipid monomers through the aqueous phase (Eq. (1)) and (ii) lipid exchange upon binary (Eq. (2)) or ternary (Eq. (3)) nanodisc collisions. As (i) is a saturable process, it plays an important role only at low lipid concentration, c_{L}. By contrast, (ii) gives rise to a second-order and, possibly, even third-order kinetic process that dominates at higher c_{L}. We utilised TR-FRET to dissect the contributions of these mechanisms to the exchange of phospholipid

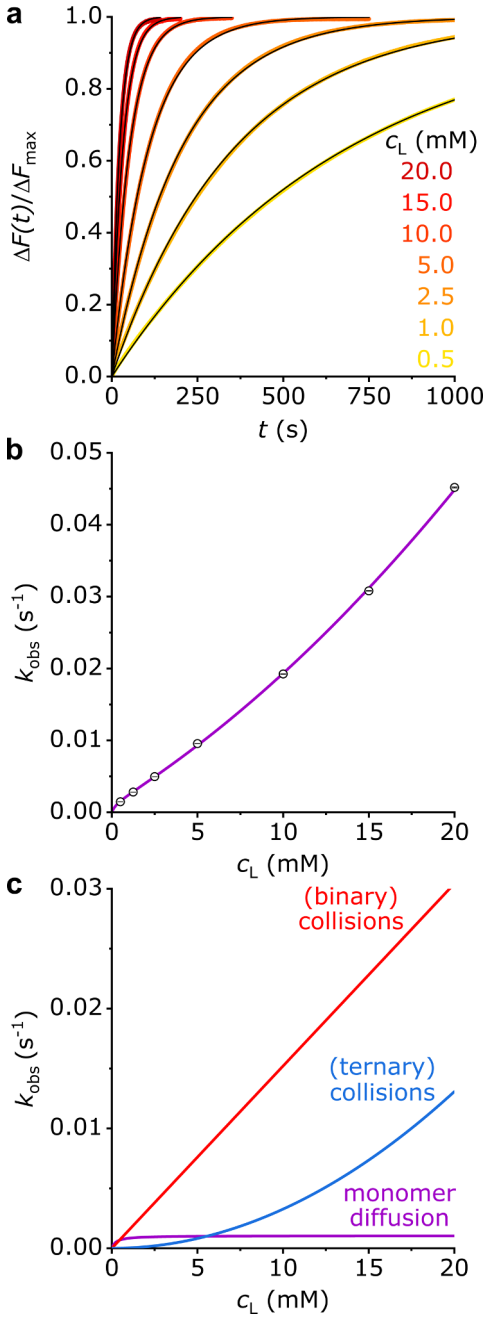

Fig. 1. Lipid transfer among fluorescently labelled and unlabelled DIBMALPs at c_{NaCl} = 200 mM and 30 °C as monitored by TR-FRET. (a) Normalised NBD-PE fluorescence intensity, $\Delta F(t)/\Delta F_{max}$, versus time, t, upon mixing labelled DIBMALPs at final c_L° = 0.25 mM with unlabelled DIBMALPs at final c_L = 0.5–20 mM. Shown are experimental data (coloured dots) and a global fit (black lines) based on Eq. (6). (b) Observed transfer rate constants derived from experimental traces in panel a. Data points are from local fits (circles) and a global fit (purple line) as derived from Eqs. (5) and (6), respectively. Error bars (within circles) represent 95% confidence intervals from local fits. (c) Contributions from diffusional and collisional lipid-exchange processes to k_{obs} as derived from Eq. (4). (For interpretation of the references to colour in this figure legend, the reader is referred to the web version of this article.)

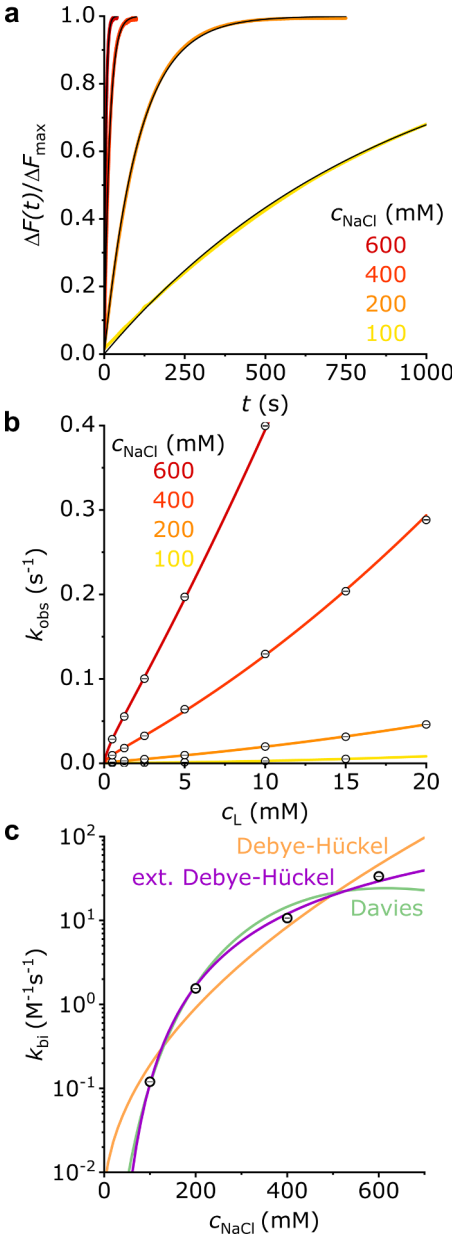

Fig. 2. Lipid transfer among fluorescently labelled and unlabelled DIBMALPs at various ionic strengths, I, at 30 °C as monitored by TR-FRET. (a) Normalised NBD-PE fluorescence intensity, $\Delta F(t)/\Delta F_{max}$, versus time, t, upon mixing labelled DIBMALPs at final c_L = 0.25 mM with unlabelled DIBMALPs at final c_L = 5 mM and c_{NaCl} = 100–600 mM. Shown are experimental data (coloured dots) and global fits (black lines) to complete datasets at each ionic strength based on Eq. (6). (b) Observed transfer rate constants, k_{obs}, as functions of c_{NaCl} from local fits according to Eq. (5) (circles) and global fits according to Eq. (6) (solid lines). Error bars (within circles) correspond to 95% confidence intervals of local fits. (c) Binary collisional transfer rate constants, k_{bi}, derived from global fits shown in panel b as functions of c_{NaCl}. Shown are experimental data (circles) and corresponding fits based on Eq. (9) (orange line), Eq. (11) (green line), or Eq. (13) (purple line). Error bars (within circles) are 95% confidence intervals of k_{bi} values. (For interpretation of the references to colour in this figure legend, the reader is referred to the web version of this article.)

molecules among DIBMALPs at various c_L values. To this end, we produced fluorescently labelled DIBMALPs consisting of a DMPC matrix hosting 1 mol% of each NBD-PE and Rh-PE as donor and acceptor fluorophores, respectively. When co-localised within the same nanodisc, NBD-PE and Rh-PE form an efficient FRET pair. Redistribution of fluorescent lipids, however, will dequench the donor and, thus, result in an increase in fluorescence emission intensity from NBD-PE.

Indeed, when we mixed labelled and unlabelled DIBMALPs at various c_L, we observed a strong increase in NBD-PE emission in a time- and concentration-dependent manner (Fig. 1a). By fitting each trace individually using Eq. (5), we found $k_{obs}(c_L)$ to exhibit negative curvature at low c_L and positive curvature at high c_L (Fig. 1b). Accounting

Table 1
Best-fit values of diffusional rate constants, k_{dif}, binary collisional rate constants, k_{bi}, ternary collisional rate constants, k_{ter}, with corresponding 95% confidence intervals as well as apparent lipid-transfer efficiencies of binary collisions, $k_{bi}^{*}/k_{bi,max}$, for DMPC nanodiscs bounded by DIBMA, SMA(2:1), or SMA(3:1) at various c_{NaCl} and d_z.

Polymer	c_{NaCl} (mM)	d_z (nm)	k_{dif} (s^{-1})	k_{bi} ($M^{-1}s^{-1}$)	k_{ter} ($M^{-2}s^{-1}$)	$k_{bi}^{*}/k_{bi,max}$ (%)
DIBMA (this work)	100	~23	$2.2 \times 10^{-4} \pm 1 \times 10^{-6}$	0.12 ± 0.001	13.9 ± 0.1	0.001
	200		$1.0 \times 10^{-3} \pm 5 \times 10^{-6}$	1.5 ± 0.004	35.1 ± 0.3	0.02
	400		$5.9 \times 10^{-3} \pm 4 \times 10^{-5}$	10.7 ± 0.03	159.3 ± 2.3	0.14
	600		$1.7 \times 10^{-2} \pm 1 \times 10^{-4}$	33.5 ± 0.07	433.3 ± 5.9	0.43
	200	~32	$6.6 \times 10^{-4} \pm 5 \times 10^{-6}$	1.4 ± 0.005	13.6 ± 0.3	0.07
	200	~40	$8.2 \times 10^{-4} \pm 8 \times 10^{-6}$	1.0 ± 0.006	131.1 ± 0.6	0.12
SMA(2:1) [24]	50	~24	$2.4 \times 10^{-4} \pm 2 \times 10^{-5}$	0.37 ± 0.24	–	0.01
	100		$9.3 \times 10^{-4} \pm 7 \times 10^{-6}$	1.3 ± 0.004	–	0.02
	200		$3.9 \times 10^{-3} \pm 3 \times 10^{-5}$	5.9 ± 0.03	–	0.1
	400		$1.5 \times 10^{-2} \pm 1 \times 10^{-4}$	21 ± 0.1	–	0.3
SMA(3:1) [21]	200		$2.9 \times 10^{-1} \pm 5 \times 10^{-3}$	222 ± 1	–	0.4

Table 2
Best-fit values of effective charge numbers, z, and hypothetical lipid-transfer rate constants of binary collisions at vanishing I, k_{col}^{0}, and corresponding 95% confidence intervals for DMPC nanodiscs encapsulated by DIBMA or SMA(2:1) as derived from the Debye–Hückel limiting law (Eq. (9)), the Davies equation (Eq. (11)), and the extended Debye–Hückel equation (Eq. (13)).

Model	DIBMA (this work)		SMA(2:1) [24]	
	z	k_{bi}^{0}	z	k_{bi}^{0}
Debye–Hückel	−2.2	4.2×10^{-3}	−2.0 ± 0.7	0.053
	(−3.0–−1.0)	(1.6×10^{-5}–1.2)		(0.003–0.95)
Davies	−4.9	4.9×10^{-7}	−3.6 ± 0.4	0.002
	(−5.9–−3.5)	(2.4×10^{-10}–9.8×10^{-4})		(0.0004–0.01)
Extended Debye–Hückel	−46.7	2.1×10^{-54}	−33 ± 11	4.6×10^{-26}
	(−51.6–−41.4)	(3.5×10^{-66}–9.1×10^{-43})		(2.1×10^{-42}–1.1×10^{-9})

for all of the above-mentioned mechanisms in a global fit (Eq. (6)) demonstrated that, at 200 mM NaCl and for DIBMALPs having a diameter of ~23 nm, monomer diffusion as well as binary and ternary collisions contributed to lipid exchange. Dissecting the contributions from the different mechanisms to k_{obs} (Fig. 1c) revealed that diffusional transfer played a significant role only at low lipid concentrations of $c_L < 1$ mM, whereas ternary collisions became important only at much higher concentrations of about $c_L \geq 10$ mM.

The diffusional transfer rate constant, k_{dif}, amounted to 0.001 s^{-1}, which is ~4 and ~300 times lower than among SMA(2:1)- [24] and SMA(3:1)-bounded nanodiscs [21], respectively. Importantly, the desorption of lipid molecules from the bilayer membrane is known to be the rate-limiting step in diffusional lipid transfer [32,35,46]. Thus, our results imply a well-preserved lipid-bilayer core in DIBMALPs, which increases the free-energy barrier considerably and slows down diffusional transfer. Accordingly, SMA(2:1)-encapsulated nanodiscs preserve the lipid bilayer almost equally well, whereas SMA(3:1) adversely affects the lipid-bilayer structure and, therefore, facilitates diffusional lipid exchange. This interpretation receives strong support from results obtained by differential scanning calorimetry [1,6,25] and small-angle X-ray scattering (SAXS) [2,47], which show that DIBMA has milder effects than SMA(2:1) and, in particular, SMA(3:1) on the thermotropic gel-to-fluid phase transition and the bilayer architecture of nanodiscs, respectively.

The transfer rate constant characterising lipid exchange upon binary DIBMALP collisions, $k_{bi} = 1.5\ M^{-1}s^{-1}$, was found to be ~4 times and ~150 times lower than for SMA(2:1) [24] and SMA(3:1) [21], respectively. Of these three copolymers, DIBMA carries the highest negative charge, as it contains 50 mol% maleic acid, whereas SMA(2:1) and SMA(3:1) have maleic acid contents of 33 mol% and 25 mol%, respectively. Therefore, collisional transfer among DIBMALPs is expected to be slower than among SMALPs. In addition to diffusional lipid transfer and content exchange through binary collisions, we observed a significant contribution of ternary collisions to k_{obs}, which manifested in a third-order rate constant of $k_{ter} = 35.1\ M^{-2}s^{-1}$. This markedly contrasts with lipid transfer among both SMA(2:1)- and SMA(3:1)-bounded nanodiscs, where only binary collisions are discernible [21,24]. As ternary collisions play an increasing role at higher c_L, this mechanism might, in principle, apply to SMALPs as well but may be camouflaged by faster exchange through binary collisions across the range of c_L values tested for SMA.

4.2. Role of Coulombic repulsion

The polymer rim of each DIBMALP contains some hundred carboxylate groups, which confer a high negative charge to the nano-disc. Increasing the ionic strength reduces the effective charge on these carboxylate groups and, thus, should enhance collisional transfer among DIBMALPs. Hence, we measured lipid transfer among DIBMALPs by TR-FRET in the presence of 100, 200, 400, and 600 mM NaCl. As expected, we observed faster lipid exchange with increasing c_{NaCl} at a given c_L (Fig. 2a). Both local (Eq. (5)) and global fits (Eq. (6)) to the experimental data consistently furnished monotonically increasing $k_{obs}(c_{NaCl})$ values (Fig. 2b). Best-fit values and corresponding 95% confidence intervals for k_{dif}, k_{bi}, and k_{ter} are summarised in Table 1.

To rationalise the salt effect on the lipid-transfer kinetics characterising binary collisions, we fitted k_{bi} as a function of ionic strength, I. In doing so, we adopted (i) the Debye–Hückel limiting law (Eq. (9)), which is, in general, only valid for low I; (ii) the Davies equation (Eq. (11)), an empirical extension applicable to higher I, and (iii) an extended version of the Debye–Hückel equation (Eq. (13)) that accounts for the finite size of the colliding charged particles (Fig. 2c). The Debye–Hückel limiting law reproduced the experimental data only insufficiently, as has already been observed for SMA(2:1) nano-discs [24]. Although the Davies equation afforded better agreement between experiment and fit, the resulting charge number amounting to $z = -4.9$ is unrealistically small. Rather than reflecting the "true" charge of a

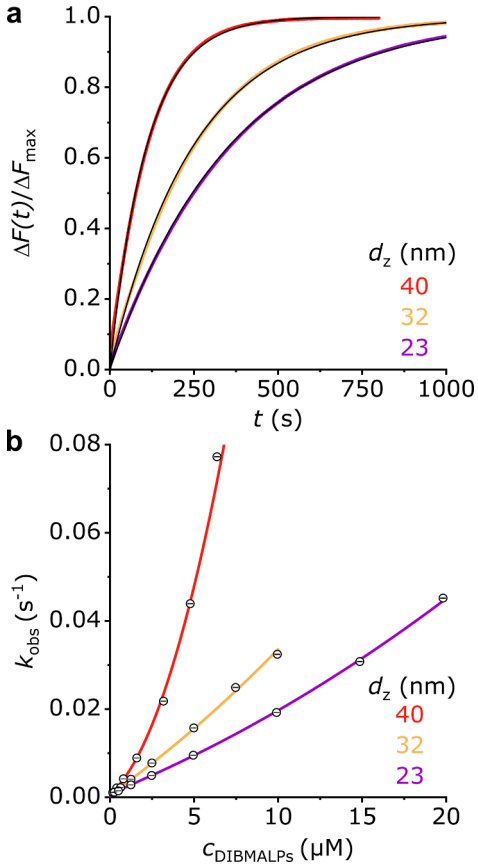

Fig. 3. Lipid transfer among fluorescently labelled and unlabelled DIBMALPs at various nanodisc diameters, d_z, at 30 °C and 200 mM NaCl as monitored by TR-FRET. (a) Normalised NBD-PE fluorescence intensity, $\Delta F(t)/\Delta F_{max,}$ versus time, t, upon mixing labelled DIBMALPs at final $c_{DIBMALP} \approx 0.15$ μM with unlabelled DIBMALPs at final $c_{DIBMALP} \approx 1.5$ μM. Shown are experimental data (coloured dots) and global fits (black lines) from complete datasets at each d_z based on Eq. (6). (b) Observed transfer rate constants, k_{obs}, as functions of $c_{DIBMALP}$ for different nanodisc sizes derived by local (circles) or global (lines) fits according to Eqs. (5) and (6), respectively. Error bars (within circles) correspond to 95% confidence intervals of local fits. (For interpretation of the references to colour in this figure legend, the reader is referred to the web version of this article.)

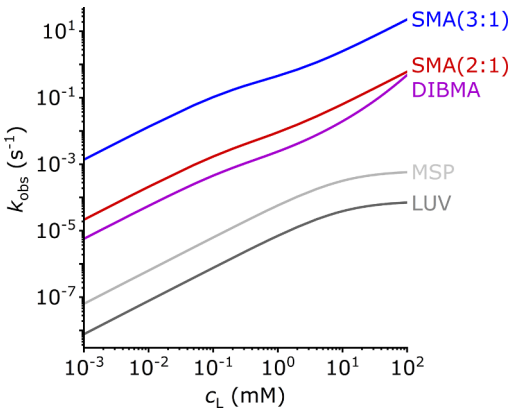

Fig. 4. Observed lipid-transfer rate constants, k_{obs}, as functions of lipid concentration, c_L, as determined for DIBMALPs (this work), nanodiscs encapsulated by SMA(2:1) [24], SMA(3:1) [21], or MSP [23], and LUVs [22]. All membrane mimics contained a DMPC matrix. Polymer-bounded nanodiscs were measured at 30 °C and 200 mM NaCl. MSP nanodiscs and LUVs were measured at 27 °C and 150 mM NaCl.

DIBMALP, this value should be taken to represent a hypothetical point charge that would show the same dependence on ionic strength as we observed for DIBMALPs.

By contrast, avoiding the point-charge approximation by use of another extension of the Debye–Hückel equation (Eq. (13)) yielded $z = -46.7$, which is considerably more negative than $z = -33$ determined analogously for SMA(2:1)-encapsulated nanodiscs [24]. Although these values are still an order of magnitude lower than the respective nominal values for DIBMALPs and SMALPs, they appear to be reasonable estimates of the effective charges, given that two colliding nanodiscs "sense" only those charged groups that are close to the region of impact. Moreover, it should be kept in mind that the current model assumes the colliding particles to be spherical with a uniform charge density, whereas polymer-bounded nanodiscs are discoidal structures with a zwitterionic lipid-bilayer patch surrounded by a highly anionic rim [1,2]. The model is further limited because the contributions of DIBMA itself and of its counterions to the total ionic strength were not explicitly accounted for. However, correcting the ionic-strength values by assuming various degrees of DIBMA ionisation did not significantly affect z, as such changes were almost fully absorbed by k_{bi}^0 (data not shown). Table 2 summarises all best-fit values and corresponding 95% confidence intervals of z and k_{bi}^0 obtained on the basis of the above three models.

4.3. Role of nanodisc size

According to the Einstein–Stokes–Smoluchowski equation, the frequency of collisions among nonionic particles at a given temperature is determined solely by the viscosity of the solvent and, in particular, does not depend on particle size [45]. In the case of polymer-based nanodiscs, however, changes in particle size are coupled to (and made possible by) shifts in the polymer/lipid ratio, which will affect the number, density, and arrangement of charges (i.e., deprotonated carboxylate groups). To investigate the consequences of this effect for collisional lipid transfer, we repeated the above experiments in the presence of 200 mM NaCl using larger DIBMALPs having hydrodynamic diameters of $d_z = 32$ and 40 nm. To allow for a fair comparison among nanodiscs containing various numbers of lipid molecules, fitted values derived from Eqs. (1)–(6), which are based on a lipid concentration scale, were converted to values referring to a nanodisc concentration scale [21]. For this purpose, we estimated DIBMALPs of $d_z = 23$, 32, and 40 nm to harbour ~1000, ~2000, and ~3100 lipid monomers, respectively.

At each DIBMALP concentration, $c_{DIBMALP}$, we observed that collisional lipid transfer became faster with increasing particle size (Fig. 3a). Again, this was borne out quantitively by both local (Eq. (5)) and global fits (Eq. (6)) to the experimental data (Fig. 3b). Table 1 summarises best-fit values and 95% confidence intervals of k_{dif}, k_{bi}, and k_{ter}. Although larger DIBMALPs overall are more charged than smaller ones, they have a lower polymer/lipid ratio and, thus, a smaller charge density. This means that, here too, it is not the absolute charge but rather the charge density that is decisive for collisional lipid transfer. Accordingly, a lower charge density as found in larger nanodiscs diminishes Coulombic repulsion and, therefore, facilitates collisional lipid transfer. It should be noted that larger DIBMALPs retain vesicle-like thermotropic phase-transition properties of DMPC bilayers better than smaller ones do [25]. Consequently, the observed acceleration of lipid exchange with increasing DIBMALP size cannot be ascribed to looser lipid packing in larger nanodiscs.

4.4. Comparison of lipid-transfer kinetics with other membrane mimics

It is instructive to calculate the lipid-transfer efficiency by comparing k_{bi}^*, which is referenced to the concentration of nanodiscs, $c_{DIBMALP}$, rather than c_L, to the highest possible value that is limited only by DIBMALP diffusion, which would amount to

$k_{bi,max}$ = (8.3–7.9) × 10^9 M^{-1} s^{-1} for nonionic particles diffusing in an aqueous solution containing 100–600 mM NaCl at 30 °C (Eq. (14)) [45]. Accordingly, the transfer efficiency of DIBMALPs with diameters of ~23 nm increased from ~0.001% at 100 mM NaCl to 0.43% at 600 mM NaCl. The apparent lipid-transfer efficiencies of DIBMALPs thus are similar to that of TX-100 micelles with ~0.02% [48] but are consistently lower than those determined for SMA(2:1) with ~0.01–0.3% at 50–400 mM NaCl [24] and SMA(3:1) with ~0.4% at 200 mM NaCl [21]. Moreover, a 6-fold increase in ionic strength enhanced the lipid-transfer efficiency among DIBMALPs ~300-fold, whereas an 8-fold increase in ionic strength has been found to result in an only 30-fold enhancement in the case of SMA(2:1)-bounded nanodiscs. Both the lower absolute values of the lipid-transfer efficiency among DIBMALPs as well as their stronger dependence on ionic strength are readily explained by the higher charge density of DIBMA as compared with the more hydrophobic SMA copolymers.

In order to enable quantitative comparisons of overall lipid-transfer rates across various membrane-mimetic systems, we added the present k_{obs} values measured for DIBMALPs to a compilation of literature values reported for a range of other colloidal membrane models (Fig. 4) [21–24]. Although DIBMALPs exchange lipids more slowly than nanodiscs encapsulated by SMA(2:1) [24] or SMA(3:1) [21], lipid transfer is still much faster than among conventional membrane mimics such as LUVs [22] and MSP nanodiscs [23]. As we have previously found for other polymer-bounded nanodiscs, lipid transfer among DIBMALPs takes place on timescales of seconds to minutes at lipid concentrations typically used for *in vitro* experiments. No information is currently available on the lipid-exchange kinetics among DIBMALPs harbouring membrane proteins or complex lipid extracts from cellular membranes. Given the collision-based mechanism resulting in *en masse* lipid transfer found here, however, it appears highly unlikely that the mere presence of proteins or a more complex lipid composition *per se* could suppress fast lipid exchange among DIBMALPs. Hence, the enrichment or depletion of certain lipid species in protein-containing vs. protein-free DIBMALPs points to the existence of strong protein/lipid interactions, as loosely bound lipids could readily exchange between both kinds of nanodiscs [20].

5. Conclusions

We have demonstrated that lipid transfer among DIBMALPs

- is slower than among nanodiscs bounded by SMA(2:1) or SMA(3:1) but substantially faster than among LUVs or MSP nanodiscs;
- is dominated by binary and ternary collisions at millimolar lipid concentrations, whereas diffusional transfer plays a significant role only at lower concentrations;
- becomes substantially faster with ionic strength, as best described by an extension of the Debye–Hückel equation, provided that z is taken as the effective rather than the nominal charge number;
- becomes considerably faster with nanodisc size, as the charge density on larger DIBMALPs is lower than that on smaller ones.

Conflicts of interest

None.

Acknowledgments

Anne Grethen (TUK) is gratefully acknowledged for assistance with TR-FRET experiments and helpful advice. We thank Erik Frotscher, Johannes Klingler, Florian Mahler, and Dr. Carolyn Vargas (all TUK) for fruitful discussions. This work was supported by the Carl Zeiss Foundation through the Centre for Lipidomics (CZSLip) and the Deutsche Forschungsgemeinschaft (DFG) through International Research Training Group (IRTG) 1830.

References

[1] A.O. Oluwole, B. Danielczak, A. Meister, J.O. Babalola, C. Vargas, S. Keller, Solubilization of membrane proteins into functional lipid-bilayer nanodiscs using a diisobutylene/maleic acid copolymer, Angew. Chem. Int. Ed. 56 (2017) 1919–1924.
[2] A.O. Oluwole, J. Klingler, B. Danielczak, J.O. Babalola, C. Vargas, G. Pabst, S. Keller, Formation of lipid-bilayer nanodiscs by diisobutylene/maleic acid (DIBMA) copolymer, Langmuir 33 (2017) 14378–14388.
[3] S.R. Tonge, B.J. Tighe, Responsive hydrophobically associating polymers: a review of structure and properties, Adv. Drug Deliv. Rev. 53 (2001) 109–122.
[4] T.J. Knowles, R. Finka, C. Smith, Y.-P. Lin, T. Dafforn, M. Overduin, Membrane proteins solubilized intact in lipid containing nanoparticles bounded by styrene maleic acid copolymer, J. Am. Chem. Soc. 131 (2009) 7484–7485.
[5] S.C.L. Hall, C. Tognoloni, J. Charlton, É.C. Bragginton, A.J. Rothnie, P. Sridhar, M. Wheatley, T.J. Knowles, T. Arnold, K.J. Edler, T.R. Dafforn, An acid-compatible co-polymer for the solubilization of membranes and proteins into lipid bilayer-containing nanoparticles, Nanoscale 10 (2018) 10609–10619.
[6] M.C. Orwick, P.J. Judge, J. Procek, L. Lindholm, A. Graziadei, A. Engel, G. Gröbner, A. Watts, Detergent-free formation and physicochemical characterization of nanosized lipid-polymer complexes: Lipodisq, Angew. Chem. Int. Ed. 51 (2012) 4653–4657.
[7] J.M. Dörr, S. Scheidelaar, M.C. Koorengevel, J.J. Dominguez, M. Schäfer, C.A. van Walree, J.A. Killian, The styrene-maleic acid copolymer: a versatile tool in membrane research, Eur. Biophys. J. 45 (2016) 3–21.
[8] M. Orwick-Rydmark, J.E. Lovett, A. Graziadei, L. Lindholm, M.R. Hicks, A. Watts, Detergent-free incorporation of a seven-transmembrane receptor protein into nanosized bilayer Lipodisq particles for functional and biophysical studies, Nano Lett. 12 (2012) 4687–4692.
[9] J.M. Dörr, M.C. Koorengevel, M. Schäfer, A.V. Prokofyev, S. Scheidelaar, E.A.W. van der Cruijsen, T.R. Dafforn, M. Baldus, J.A. Killian, Detergent-free isolation, characterization, and functional reconstitution of a tetrameric K^+ channel: the power of native nanodiscs, Proc. Natl. Acad. Sci. U. S. A. 111 (2014) 18607–18612.
[10] B. Bersch, J.M. Dörr, A. Hessel, J.A. Killian, P. Schanda, Proton-detected solid-state NMR spectroscopy of a zinc diffusion facilitator protein in native nanodiscs, Angew. Chem. Int. Ed. 56 (2017) 2508–2512.
[11] J. Broecker, B.T. Eger, O.P. Ernst, Crystallogenesis of membrane proteins mediated by polymer-bounded lipid nanodiscs, Structure 25 (2017) 384–392.
[12] M. Parmar, S. Rawson, C.A. Scarff, A. Goldman, T.R. Dafforn, S.P. Muench, V.L.G. Postis, Using a SMALP platform to determine a sub-nm single particle cryo-EM membrane protein structure, Biochim. Biophys. Acta 2017 (1860) 378–383.
[13] C. Sun, S. Benlekbir, P. Venkatakrishnan, Y. Wang, S. Hong, J. Hosler, E. Tajkhorshid, J.L. Rubinstein, R.B. Gennis, Structure of the alternative complex III in a supercomplex with cytochrome oxidase, Nature 557 (2018) 123–126.
[14] C. Logez, M. Damian, C. Legros, C. Dupré, M. Guéry, S. Mary, R. Wagner, C. M'Kadmi, O. Nosjean, B. Fould, J. Marie, J.-A. Fehrentz, J. Martinez, G. Ferry, J.A. Boutin, J.-L. Banères, Detergent-free isolation of functional G protein-coupled receptors into nanometric lipid particles, Biochemistry 55 (2016) 38–48.
[15] M. Jamshad, J. Charlton, Y.-P. Lin, S.J. Routledge, Z. Bawa, T.J. Knowles, M. Overduin, N. Dekker, T.R. Dafforn, R.M. Bill, D.R. Poyner, M. Wheatley, G-protein coupled receptor solubilization and purification for biophysical analysis and functional studies, in the total absence of detergent, Biosci. Rep. 35 (2015).
[16] M. Damian, V. Pons, P. Renault, C. M'Kadmi, B. Delort, L. Hartmann, A.I. Kaya, M. Louet, D. Gagne, K.B.H. Salah, S. Denoyelle, GHSR-D2R heteromerization modulates dopamine signaling through an effect on G protein conformation, Proc. Natl Acad. Sci. U. S. A. 115 (17) (2018) 4501–4506.
[17] S. Gulati, M. Jamshad, T.J. Knowles, K.A. Morrison, R. Downing, N. Cant, R. Collins, J.B. Koenderink, R.C. Ford, M. Overduin, I.D. Kerr, T.R. Dafforn, A.J. Rothnie, Detergent-free purification of ABC (ATP-binding-cassette) transporters, Biochem. J. 461 (2014) 269–278.
[18] G. Hazell, T. Arnold, R.D. Barker, L.A. Clifton, N.-J. Steinke, C. Tognoloni, K.J. Edler, Evidence of lipid exchange in styrene maleic acid lipid particle (SMALP) nanodisc systems, Langmuir 32 (2016) 11845–11853.
[19] R. Cuevas Arenas, J. Klingler, C. Vargas, S. Keller, Influence of lipid bilayer properties on nanodisc formation mediated by styrene/maleic acid copolymers, Nanoscale 8 (2016) 15016–15026.
[20] V. Schmidt, J.N. Sturgis, Modifying styrene-maleic acid co-polymer for studying lipid nanodiscs, Biochim. Biophys. Acta 2018 (1860) 777–783.
[21] R. Cuevas Arenas, B. Danielczak, A. Martel, L. Porcar, C. Breyton, C. Ebel, S. Keller, Fast collisional lipid transfer among polymer-bounded nanodiscs, Sci. Rep. 7 (2017) 45875.
[22] M. Nakano, M. Fukuda, T. Kudo, H. Endo, T. Handa, Determination of interbilayer and transbilayer lipid transfers by time-resolved small-angle neutron scattering, Phys. Rev. Let. 98 (2007) 238101.
[23] M. Nakano, M. Fukuda, T. Kudo, M. Miyazaki, Y. Wada, N. Matsuzaki, Static and dynamic properties of phospholipid bilayer nanodiscs, J. Am. Chem. Soc. 131 (2009) 8308–8312.
[24] A. Grethen, D. Glueck, S. Keller, Role of Coulombic repulsion in collisional lipid transfer among SMA(2:1)-bounded nanodiscs, J. Membr. Biol. 251 (2018) 443–451.
[25] A. Grethen, A.O. Oluwole, B. Danielczak, C. Vargas, S. Keller, Thermodynamics of nanodisc formation mediated by styrene/maleic acid (2:1) copolymer, Sci. Rep. 7 (2017) 11517.
[26] K.A. Morrison, A. Akram, A. Mathews, Z.A. Khan, J.H. Patel, C. Zhou, D.J. Hardy, C. Moore-Kelly, R. Patel, V. Odiba, T.J. Knowles, M.-U.-H. Javed, N.P. Chmel, T.R. Dafforn, A.J. Rothnie, Membrane protein extraction and purification using

styrene-maleic acid (SMA) copolymer: effect of variations in polymer structure, Biochem. J. 473 (2016) 4349–4360.
[27] D.J.K. Swainsbury, S. Scheidelaar, N. Foster, R. van Grondelle, J.A. Killian, M.R. Jones, The effectiveness of styrene-maleic acid (SMA) copolymers for solubilisation of integral membrane proteins from SMA-accessible and SMA-resistant membranes, Biochim. Biophys. Acta 2017 (1859) 2133–2143.
[28] D.E. Koppel, Analysis of macromolecular polydispersity in intensity correlation spectroscopy: the method of cumulants, J. Chem. Phys. 57 (1972) 4814–4820.
[29] G. Kemmer, S. Keller, Nonlinear least-squares data fitting in Excel spreadsheets, Nat. Prot. 5 (2010) 267–281.
[30] J.W. Nichols, R.E. Pagano, Kinetics of soluble lipid monomer diffusion between vesicles, Biochemistry 20 (2001) 2783–2789.
[31] J.W. Nichols, R.E. Pagano, Use of resonance energy transfer to study the kinetics of amphiphile transfer between vesicles, Biochemistry 21 (2002) 1720–1726.
[32] J.W. Nichols, Thermodynamics and kinetics of phospholipid monomer-vesicle interaction, Biochemistry 24 (1985) 6390–6398.
[33] J.W. Nichols, Phospholipid transfer between phosphatidylcholine-taurocholate mixed micelles, Biochemistry 27 (1988) 3925–3931.
[34] D.A. Fullington, D.G. Shoemaker, J.W. Nichols, Characterization of phospholipid transfer between mixed phospholipid-bile salt micelles, Biochemistry 29 (1990) 879–886.
[35] J.D. Jones, T.E. Thompson, Mechanism of spontaneous, concentration-dependent phospholipid transfer between bilayers, Biochemistry 29 (1990) 1593–1600.
[36] D.A. Fullington, J.W. Nichols, Kinetic analysis of phospholipid exchange between phosphatidylcholine/taurocholate mixed micelles: effect of the acyl chain moiety of the micellar phosphatidylcholine, Biochemistry 32 (1993) 12678–12684.
[37] J.N. Brønsted, Zur Theorie der chemischen Reaktionsgeschwindigkeit, Z. Phys. Chem. 102 (1922) 169–207.
[38] J.N. Brønsted, C.E. Teeter, On kinetic salt effect, J. Phys. Chem. 28 (6) (1923) 579–587.
[39] N.J. Bjerrum, Zur Theorie der chemischen Reaktionsgeschwindigkeit, Z. Phys. Chem. 108 (1924) 82–100.
[40] P. Debye, E. Hückel, Zur Theorie der Elektrolyte. I. Gefrierpunktserniedrigung und verwandte Erscheinungen, Phys. Z. 24 (1923) 185–206.
[41] P.R. Bergethon, The Physical Basis of Biochemistry: The Foundations of Molecular Biophysics, 2nd. ed., Springer, New York, 2010.
[42] E.A. Guggenheim, L., The specific thermodynamic properties of aqueous solutions of strong electrolytes, Phil. Mag. 19 (1935) 588–643.
[43] C.W. Davies, 397. The extent of dissociation of salts in water. Part VIII. An equation for the mean ionic activity coefficient of an electrolyte in water, and a revision of the dissociation constants of some sulphates, J. Chem. Soc. (1938) 2093–2098.
[44] C.W. Davies, Ion Association, Butterworth, Washington, D.C. 1962.
[45] J. Kuriyan, B. Konforti, D. Wemmer, The Molecules of Life: Physical and Chemical Principles, Garland Science, New York, 2013.
[46] E.A.G. Aniansson, S.N. Wall, M. Almgren, H. Hoffmann, I. Kielmann, W. Ulbricht, R. Zana, J. Lang, C. Tondre, Theory of the kinetics of micellar equilibria and quantitative interpretation of chemical relaxation studies of micellar solutions of ionic surfactants, J. Phys. Chem. 80 (1976) 905–922.
[47] M. Jamshad, V. Grimard, I. Idini, T.J. Knowles, M.R. Dowle, N. Schofield, P. Sridhar, Y. Lin, R. Finka, M. Wheatley, O.R.T. Thomas, R.E. Palmer, M. Overduin, C. Govaerts, J.-M. Ruysschaert, K.J. Edler, T.R. Dafforn, Structural analysis of a nanoparticle containing a lipid bilayer used for detergent-free extraction of membrane proteins, Nano Res. 8 (2015) 774–789.
[48] Y. Rharbi, M. Li, M.A. Winnik, K.G. Hahn, Temperature dependence of fusion and fragmentation kinetics of Triton X-100 micelles, J. Am. Chem. Soc. 122 (2000) 6242–6251.